Air stable all-inorganic nanocrystal solar cells processed from solution

Ilan Gur[*,1,3], Neil A. Fromer[1], Michael L. Geier[1], and A. Paul Alivisatos[1,2]

[1]Material Science Division, Lawrence Berkeley National Laboratory, Berkeley CA 94720

[2]Department of Chemistry, University of California, Berkeley CA 94720

[3]Department of Materials Science and Engineering, University of California, Berkeley CA 94720

* To whom correspondence should be addressed. Email:igur@berkeley.edu

We introduce an ultrathin donor-acceptor solar cell comprised entirely of inorganic nanocrystals spin-cast from solution. These devices are stable in air, and post-fabrication processing allows for power conversion efficiencies approaching 3% in initial tests. This demonstration elucidates a new class of photovoltaic device with potential for stable, low cost power generation.

Small molecule and polymer organic solar cells are promising candidates for affordable wide-scale solar energy conversion, but while organic materials offer strong potential for cost reduction vis-à-vis conventional solar cells, their spectrally limited absorption and low carrier mobilities impose limitations to achieving commercially viable device efficiencies (*1*). Colloidal inorganic nanocrystals share all of the primary advantages of organics - scalable and controlled synthesis, an ability to be processed in solution, and a decreased sensitivity to substitutional doping – while retaining the broadband absorption and superior transport properties of traditional photovoltaic semiconductors (*2-4*). Accordingly, utilizing inorganic nanocrystals for electron transport has been found to

enhance performance in semiconducting polymer solar cells (*5, 6*). Hybrid systems have kept pace with their organic counterparts; however, it is clear that the ultimate limitations of hybrids may still be dictated by low mobility and environmental sensitivity of the remnant organic phase. A new class of solar cell based exclusively on colloidal nanocrystals has been anticipated theoretically in recent years (*7, 8*). This investigation demonstrates such a device and presents a mechanism for its operation in the context of organic donor-acceptor and conventional p-n junction solar cells.

In recent years, a well-accepted model has emerged to describe the operation of organic based solar cells and distinguish them from their conventional inorganic counterparts (*7, 9*). The organic donor-acceptor solar cell relies on a type II heterojunction, which serves to dissociate the strongly bound excitons characteristic of organic systems. Materials design for this type of photovoltaic system thus requires proper energy band alignment of active materials to facilitate charge transfer. Examples to date have been limited to systems utilizing at least one active organic component (*5, 10-14*). However, studies of type II semiconductor nanocrystal heterostructures demonstrate that efficient charge transfer may also occur between two such inorganic components with staggered energy levels (*15, 16*). In addition, recent research has revealed a growing number of similarities between films of nanocrystals and organic molecular semiconductors. As is the case with organic systems, nanocrystal films exhibit extremely low carrier concentrations and high trap densities (*17, 18*), as well as confined excitations which may migrate between crystals (*19*). All of these properties are sufficient, and some requisite, for solar energy conversion based on the donor-acceptor model (*7, 9*). The strong similarities between the

two classes of materials suggest that a nanocrystal donor-acceptor solar cell may be constructed without any organic component.

The photovoltaic devices described here utilize rod-shaped cadmium selenide (Figure 1A) and cadmium telluride (Figure 1B) nanocrystals, synthesized and prepared separately (*21*). A schematic energy diagram in Figure 1C illustrates the staggered band alignment of this prototypical donor-acceptor pair (*20*). In fabricating devices, nanocrystals were spin-cast from a filtered pyridine solution, allowing for the creation of ultra thin, flexible films of densely packed nanocrystals on virtually any substrate. In Figure 1D, a representative scanning electron micrograph shows that typical films are homogeneous and pinhole-free over large areas.

Planar donor-acceptor heterojunctions were fabricated by sequentially spin-casting films of CdTe followed by CdSe on indium tin oxide (ITO) glass. Thermally deposited aluminum was used as a reflective top contact. Brief annealing of the first film for 15 minutes at 200 degrees C was found to remove residual solvent and allow for superjacent deposition of the second film, thus creating high quality bilayer structures with minimal intermixing at the interface (*21*).

In Figure 2A, the photoaction spectrum of a typical bilayer cell reveals features from both the CdSe and CdTe absorption spectra, demonstrating that both components contribute to the photocurrent. Current-voltage characteristics of this device in the dark and at simulated AM1.5G full-sun illumination are presented in Figure 2B. The device exhibits

strong photo-response and diode rectification in the dark and light. In addition, this representative cell exhibits a significant photovoltaic effect, with short circuit current (I_{sc}) of 0.58 mA/cm^2, open circuit voltage (V_{oc}) of 0.41 V, and fill factor (FF) of 0.40 (*22*).

Given their ostensibly similar structures, it is necessary to distinguish the solar cells presented here from conventional thin film heterojunction cells. Conventional cells depend on a junction between bulk p- and n- doped materials to form a built-in field, which then acts as the primary driving force for minority carrier extraction (*23, 24*). Similar to organic semiconductors, colloidal nanocrystals are characterized by extremely limited free-carrier concentrations (*4*). In fact, three-dimensional CdSe colloid arrays have been found to contain essentially no free carriers without illumination (*18*). As such, the creation of a depleted junction in these nanocrystal cells is highly unlikely.

In accordance with prior studies, the CdSe and CdTe films presented here are electrically insulating in the dark. Measuring surface conduction across a 1mm gap between two aluminum electrodes yields linear IV curves, from which sheet resistances exceeding 500 G-ohms/□, a value limited by the measurement apparatus, can be extracted for films of either material on glass substrates. Exposing the films to 100 mw/cm2 full-sun irradiation affects a dramatic rise in conductivity. Sheet resistances, now measurable, drop at least one order of magnitude under illumination. Likewise, illumination affords a greater than three order of magnitude enhancement in conductivity of the device itself, as demonstrated in Figure 2A. This strong photoconductive effect suggests that these materials, like their organic counterparts, have an extremely limited number of untrapped

carriers in the dark, and are better characterized by a rigid band model than one employing band bending.

Accounting for these effectively undoped active materials, we propose a mechanism for photovoltaic conversion based on donor-acceptor charge transfer. Those photoexcitations that probe the CdTe/CdSe junction experience an energetic driving force for charge transfer, with holes finding lower energy states in the CdTe and electrons finding lower states in the CdSe. Carrier extraction is driven not by means of a built-in field created from a depletion region of substitutional dopants; rather, extraction is primarily driven by directed diffusion, as dictated by the type II heterojunction. After absorption and charge transfer, majority holes in the CdTe readily diffuse into the ITO, but are blocked from moving through the CdSe toward the Al electrode. Likewise, majority electrons in the CdSe can diffuse only toward the Al, and not through the CdTe to the ITO. The well-accepted metal-insulator-metal model, in which electrodes of disparate work function equilibrate to form a field across the dielectric active materials, likely provides an additional driving force for carrier extraction.

In order to assess the role of charge transfer in facilitating photovoltaic energy conversion, devices comprised of a thin-film of only one nanocrystal material were juxtaposed with cells containing charge transfer junctions between the two types of crystals. All devices had comparable thicknesses of active materials on the order of 100 nm and comparable optical densities across the spectrum. A direct comparison of external quantum efficiencies in the CdTe-only, CdSe-only, and bilayer CdTe/CdSe

devices appears in Figure 2C, showing a significant enhancement in creation and extraction of carriers due solely to the presence of a charge transfer interface within the device. As is the case in organic systems, separation of electrons and holes across the interface enhances the diffusional driving force for charge extraction while reducing the likelihood of geminate recombination within the system. Results for devices composed of intimately mixed blends of CdSe and CdTe nanocrystals also appear in Figure 2C. These blend films similarly exhibit enhanced quantum efficiencies over single-material cells, offering further evidence that the photoaction of these devices is based on a donor-acceptor junction rather than a conventional planar p-n junction (*25*).

Additional information regarding the mechanism for charge extraction can be gained from comparing the current-voltage characteristics of these various devices. It has already been noted that cells based on heterojunction bilayers exhibit good diode behavior with strong rectification. By comparison, current-voltage characterization of devices composed of only CdTe or only CdSe showed no significant rectification. We can thus deduce that the observed photovoltaic effect in the bilayer is not a result of Schottkey contacts to either material, but rather is due to the intended heterojunction.

Having ruled out the presence of conventional p-n or Shottkey junctions, it appears that the bilayer nanocrystal cell operates by means of the diffusion assisted donor-acceptor heterojunction typical of organic devices. It is important, however, to note several characteristics of the nanocrystal solar cell that set it apart from its organic-based counter parts. Perhaps most striking is the fact that while the most efficient organic solar cells are

based on distributed heterojunctions, devices based on simple blends of donor and acceptor nanocrystals (Figure 2D) neither rectify nor produce a significant photovoltage. This poor performance can be attributed to the fact that, in contrast to organic systems, common electrodes do not readily form selective contacts to either the donor or acceptor nanocrystals. Electrons and holes can be injected into either material, such that blend cells pass current in both forward and reverse bias. Incorporation of blocking layers in future cell designs may allow for further investigation of the blend system.

Another fundamental distinction of the nanocrystal system has direct consequences on the performance of these devices. While a heterojunction is nearly always required to efficiently produce free charges from excitons in organic systems, this is not the case for the nanocrystals utilized in this study. Rod shaped nanocrystals with high aspect ratios exhibit little confinement along the length of the rod (*26*). Excitations can thus dissociate over this dimension, creating free carriers throughout the nanocrystal film. This is a significant departure from organic systems, in which free carriers are created only when otherwise tightly bound excitons are separated across the donor-acceptor junction.

With both free electrons and holes residing in the donor and acceptor materials, carriers are more susceptible to non-geminate recombination in the nanocrystal system. This recombination is compounded by the large presence of surface states on the nanocrystals, which act to trap carriers as they move through the film. Indeed, detrimental recombination losses are apparent in the low quantum efficiency of the nanocrystal cell compared with similar devices made from organic semiconductors.

It is possible to minimize the high surface trap area inherent in a densely packed array of nanocrystals and concurrently improve carrier transport in the device by annealing and sintering the crystals. Following a well-known technique to facilitate sintering of CdTe thin films (*27*), nanocrystal films were exposed to a saturated solution of cadmium chloride in methanol and annealed at 400 degrees in oxygen for 15 minutes. After sintering, films of CdSe and CdTe remain insulating in the dark, but show an approximately two order of magnitude enhancement in photoconductivity. This suggests that the sintering process dramatically improves carrier transport, but does not result in significant doping.

The photo-response of sintered CdTe/CdSe bilayer cells mirrors the drastic rise in photoconductivity exhibited by the active layers. A typical photoaction spectrum appears in Figure 3A, showing external quantum efficiencies approaching 70% (*28*). As expected, the spectrum reflects a strong red-shift in the onset of photocurrent to the bulk absorption edge. With I_{sc} of 11.6 mA/cm^2, V_{oc} of 0.40 V and FF of 0.45, the resulting solar cell demonstrates a power conversion efficiency of 2.1 % under simulated AM1.5G illumination (*29*). Note that the enhancement in efficiency arises solely from the dramatic increase in photo-response, while cells exhibit a nearly unchanged open circuit voltage after sintering (Figure 3B). This is strong evidence that the driving force for charge extraction is the same in sintered and unsintered devices.

By varying simple system parameters such as electrode material, even higher efficiencies have already been achieved in sintered nanocrystal cells. Figure 3C shows current-voltage characteristics for the best device fabricated to date. Employing a calcium top contact capped with aluminum, this cell demonstrates an AM1.5G power conversion efficiency of 2.9 %, with I_{sc} of 13.2 mA/cm^2, Voc of 0.45 V and FF of 0.49.

None of the solar cells presented here, whether sintered or not, exhibited the strong sensitivity to photo-oxidation characteristic of organic-based devices; in fact, aging seems to improve rather than deteriorate their performance. Figure 4 shows the AM1.5G full-sun behavior of a typical sintered device characterized in air before and after 13,000 hours' exposure to ambient atmosphere and lighting. The cell shows only a 1.4% decrease in short-circuit current, while the fill-factor rose 4.4% and the open-circuit voltage increased by over 10%. Overall, the atmospheric aging resulted in a 13.6% increase in efficiency. Light soaking experiments revealed less than 2% degradation in photocurrent after 14 hours at short-circuit under simulated AM1.5G illumination. These phenomena serve to illustrate the robustness of this system over its organic counterparts.

This demonstration introduces the first solar cells based entirely on colloidal semiconductor nanocrystals. They are ultra-thin, solution-processed, and stable in ambient environments. Comprised of dense nanocrystal films that mirror the basic properties of semiconducting polymers, these cells function as a new class of diffusion assisted donor-acceptor heterojunction. Sintering is found to enhance the performance of these devices, allowing for air-stable power conversion efficiencies up to 2.9%. The

nanocrystal solar cells presented here offer a new research direction and serve as a key development toward achieving stable and low-cost solar energy conversion.

Figure 1

Transmission electron micrographs of (**A**) CdSe and (**B**) CdTe nanocrsytals utilized in this investigation. Scale bar, 40 nm. In (**C**), an energy diagram of valence and conduction band levels for CdTe and CdSe as calculated from the effective mass theory clearly illustrates the type II charge-transfer junction formed between the two materials. In (**D**), a typical spin-cast film of colloidal nanocrystals imaged by scanning electron microscopy is homogeneous and defect free; the film edge of this ca. 100 nm film is shown for contrast with the silicon substrate. Scale bar, 1 μm.

Figure 2

(**A**) The normalized photocurrent spectral response of a typical ITO/100 nm CdTe/100 nm CdSe/Al bilayer device (bold) is illustrated alongside solution-phase absorption spectra for the CdTe (dotted) and CdSe (solid) nanocrystals from which the device was fabricated. The photoaction spectrum reflects the red CdTe absorption edge and the prominent CdSe exciton peak, indicating that both components are active. (**B**) Current-voltage characteristics for this device in the dark (dotted) and under simulated one-sun AM1.5G illumination. The device behaves as a rectifying diode with a significant photovoltaic response. Note also the strong photoconductive response of the device. (**C**) A comparison of external quantum efficiency spectra shows significant enhancement in bilayer (bold, solid) and blend (bold, dotted) devices versus a CdTe single-material device (solid) and CdSe single-material device (dotted), all of comparable optical density. The comparison serves to illustrate the role of charge transfer in photocurrent generation. (**D**) A comparison of current-voltage characteristics between the same devices: nearly

symmetric current-voltage behavior in the single-material devices suggests that diode behavior in the bilayer is not simply the result of a Schottkey junction with either material. With no contact selectivity, blend cells show negligent rectification and photovoltage at simulated AM1.5G illumination.

Figure 3

(**A**) The normalized photo-action spectrum of a typical bilayer device after sintering reveals the broadened spectral response and enhanced quantum efficiency that result from sintering. (**B**) Current-voltage characteristics of a typical bilayer device before sintering (dotted) and after sintering (solid), measured at simulated one-sun AM1.5G illumination. The sintered cell shows over an order of magnitude enhancement in photocurrent while the open circuit voltage remains virtually unchanged. (**C**) Utilizing a Ca 20nm/Al 80nm top contact allows for fabrication of devices with AM1.5G power conversion efficiencies as high as 2.9%

Figure 4

Current-voltage behavior at simulated one-sun AM1.5G illumination for a typical sintered bilayer device upon first exposure to air (solid) and after 13000 hours exposure to ambient atmosphere and light. Exposure to air and ambient light results shows minimal degradation in short-circuit current, and ultimately affords a 13.6% improvement in overall power conversion efficiency.

Figure 1

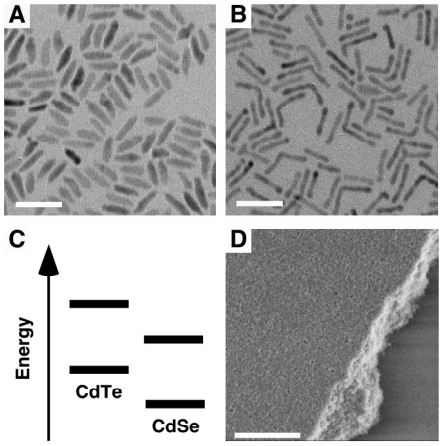

Figure 2

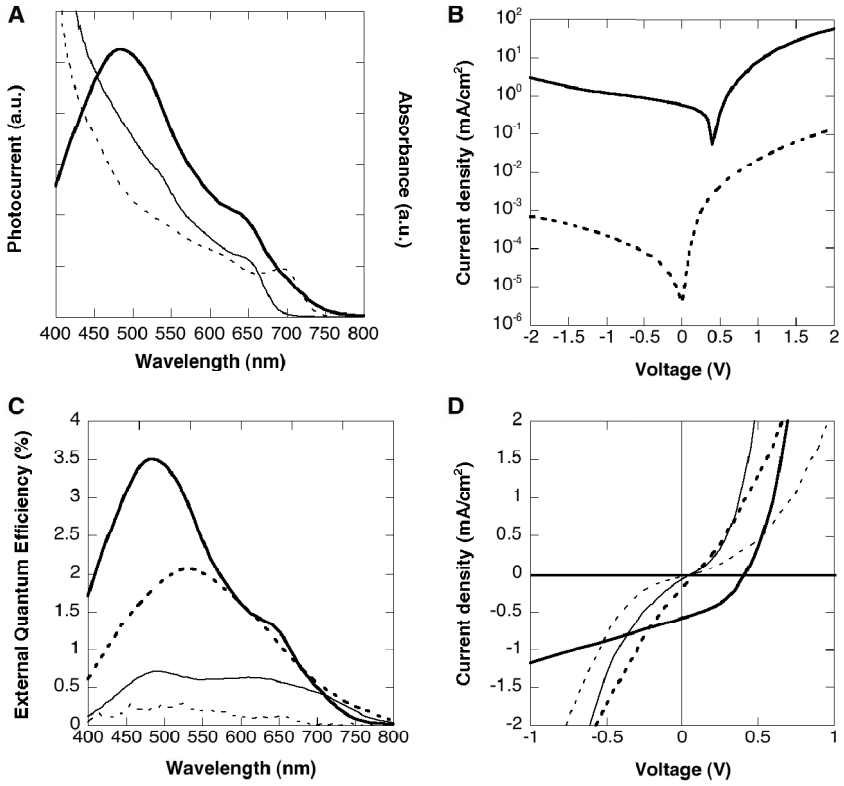
A
Photocurrent (a.u.)
Absorbance (a.u.)
400 450 500 550 600 650 700 750 800
Wavelength (nm)
B
Current density (mA/cm²)
10² 10¹ 10⁰ 10⁻¹ 10⁻² 10⁻³ 10⁻⁴ 10⁻⁵ 10⁻⁶
-2 -1.5 -1 -0.5 0 0.5 1 1.5 2
Voltage (V)
C
External Quantum Efficiency (%)
0 0.5 1 1.5 2 2.5 3 3.5 4
400 450 500 550 600 650 700 750 800
Wavelength (nm)
D
Current density (mA/cm²)
2 1.5 1 0.5 0 -0.5 -1 -1.5 -2
-1 -0.5 0 0.5 1
Voltage (V)

Figure 3

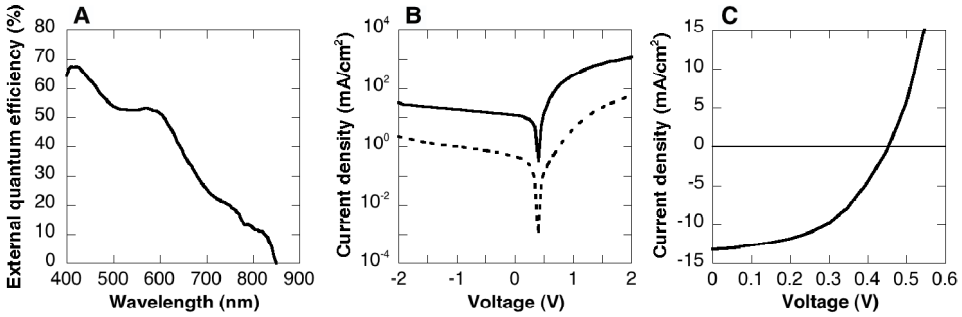
A
External quantum efficiency (%)
80
70
60
50
40
30
20
10
0
400 500 600 700 800 900
Wavelength (nm)
B
Current density (mA/cm²)
10⁴
10²
10⁰
10⁻²
10⁻⁴
-2 -1 0 1 2
Voltage (V)
C
Current density (mA/cm²)
15
10
5
0
-5
-10
-15
0 0.1 0.2 0.3 0.4 0.5 0.6
Voltage (V)

Figure 4

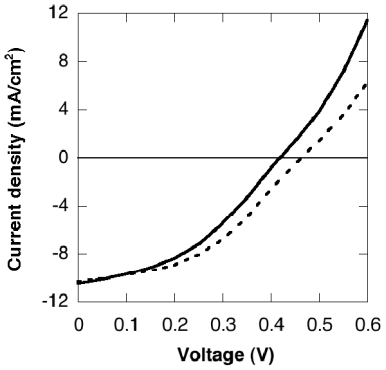

1. S. E. Shaheen, D. S. Ginley, G. E. Jabbour, *Mrs Bulletin* **30**, 10 (JAN, 2005).
2. A. P. Alivisatos, *Journal of Physical Chemistry* **100**, 13226 (AUG 1, 1996).
3. C. B. Murray, C. R. Kagan, M. G. Bawendi, *Annual Review of Materials Science* **30**, 545 (2000).
4. M. Shim, C. J. Wang, D. J. Norris, P. Guyot-Sionnest, *Mrs Bulletin* **26**, 1005 (DEC, 2001).
5. W. U. Huynh, J. J. Dittmer, A. P. Alivisatos, *Science* **295**, 2425 (MAR 29, 2002).
6. B. Q. Sun, H. J. Snaith, A. S. Dhoot, S. Westenhoff, N. C. Greenham, *Journal of Applied Physics* **97** (JAN 1, 2005).
7. B. A. Gregg, M. C. Hanna, *Journal of Applied Physics* **93**, 3605 (MAR 15, 2003).
8. A. J. Nozik, *Physica E-Low-Dimensional Systems & Nanostructures* **14**, 115 (APR, 2002).
9. J. A. Barker, C. M. Ramsdale, N. C. Greenham, *Physical Review B* **67** (FEB 15, 2003).
10. J. J. M. Halls *et al.*, *Nature* **376**, 498 (AUG 10, 1995).
11. G. Yu, J. Gao, J. C. Hummelen, F. Wudl, A. J. Heeger, *Science* **270**, 1789 (DEC 15, 1995).
12. P. Peumans, V. Bulovic, S. R. Forrest, *Applied Physics Letters* **76**, 2650 (MAY 8, 2000).
13. S. E. Shaheen *et al.*, *Applied Physics Letters* **78**, 841 (FEB 5, 2001).
14. K. M. Coakley, M. D. McGehee, *Applied Physics Letters* **83**, 3380 (OCT 20, 2003).
15. S. Kim, B. Fisher, H. J. Eisler, M. Bawendi, *Journal of the American Chemical Society* **125**, 11466 (SEP 24, 2003).
16. D. J. Milliron *et al.*, *Nature* **430**, 190 (JUL 8, 2004).
17. D. S. Ginger, N. C. Greenham, *Journal of Applied Physics* **87**, 1361 (FEB 1, 2000).
18. N. Y. Morgan *et al.*, *Physical Review B* **66** (AUG 15, 2002).
19. J. Heitmann *et al.*, *Physical Review B* **69** (MAY, 2004).
20. Employing the effective mass approximation, bulk energy levels were modified to account for quantum confinement. Electron affinities for CdSe and CdTe rods were calculated to be -4.79 and - 4.12 eV respectively. Ionization energies for CdSe and CdTe rods were calculated to be -6.64 and -5.85 eV respectively.
21. Information on materials and methods is available as supporting material on Science Online.
22. Results presented are based on devices utilizing the standardized syntheses of CdTe and CdSe described above - other syntheses have yielded slightly different results. For instance, devices with open circuit voltages as high as 0.6 have been achieved by varying nanocrystal diameter; a thorough description of this dependence will be described elsewhere.
23. S. M. Sze, *Physics of Semiconductor Devices* (John Wiley and Sons, New York, 1981), pp.
24. A. L. F. a. R. H. Bube, *Fundamentals of Solar Cells* (Academic Press, New York, 1983), pp.

25. The lower quantum efficiency of blend structures as compared with bilayers may be attributed to an increased succeptibility to non-geminate recombination.
26. L. S. Li, J. T. Hu, W. D. Yang, A. P. Alivisatos, *Nano Letters* **1**, 349 (JUL, 2001).
27. B. E. McCandless, L. V. Moulton, R. W. Birkmire, *Progress in Photovoltaics* **5**, 249 (JUL-AUG, 1997).
28. These ultrathin cells exhibit sub-optimal absorptivity, with average optical density of approximately 0.7. This assumes full back contact reflection such that incident light passes through the film twice.
29. Short-circuit currents obtained under simulated AM1.5G illumination were well matched with those obtained by integrating EQE data with the true AM1.5G solar emission spectrum. Details on solar simulation is available as supporting material on Science Online.
30. This work was supported by the Director, Office of Energy Research, Office of Science, Division of Materials Sciences, of the U.S. Department of Energy under Contract No. DE-AC02-05CH11231. I.G. further acknowledges the National Science Foundation for support under a Graduate Research Fellowship. The authors wish to offer particular thanks to the following individuals for research support and valuable discussion: Aleksandra Radenovic, Kevin Sivula, Udo Bach, Delia Milliron, James Wang, and Sarah Laubach. Dedicated in loving memory to Benjamin Boussert, Giulia Adesso, and Jason Choy.

Supporting Online Material
www.sciencemag.org
Materials and Methods

Supporting Online Material

I. Materials. Cadmium oxide (CdO) (99.99+ %), Tellurium (Te) (99.8 %, 200 mesh), Selenium (Se) (99.999%, 100 mesh), and tri-*n*-octylphosphine oxide (C24H51OP or TOPO, 99 %) were purchased from Aldrich. *n*-Octadecylphosphonic acid (C18H39O3P or ODPA), *n*-Tetradecylphosphonic acid (C14H31O3P or TDPA) and Octylphosphonic acid (C8H19O3P or OPA), *n*-Hexylphosphonic acid (C6H15O3P or HPA), were purchased from PolyCarbon Industries, Inc. Trioctylphosphine (TOP) (97 %) was purchased from Strem Chemicals. All solvents used were anhydrous, purchased from Aldrich, and used without any further purification.

II. Synthesis of CdSe and CdTe Nanorods. All manipulations were performed using standard air-free techniques. In a typical synthesis of CdSe [CdTe] rods, a mixture of 710 mg TDPA, 160 mg HPA, 3.00 g TOPO, and 200 mg CdO [812 mg ODPA, 315 mg OPA, 2.65 g TOPO, and 200 mg CdO] was degassed at 120 ºC for 60 minutes in a 25 ml three-neck flask connected to a Liebig condenser. It was heated slowly under Ar until the CdO decomposed and the solution turned clear and colorless. Next, 1.5 g of TOP were added, and the temperature was further raised to 300 ºC [320 ºC]. Next, 73 mg of selenium dissolved in 416 mg of TOP [61 mg of tellurium dissolved in 552 mg of TOP] were rapidly injected to the vigorously stirring precursors and particles were allowed to grow for 5 minutes [4 minutes] before the heat was removed to stop the reaction. After cooling the solution to 70 ºC, 3–4 ml anhydrous toluene were added to the flask, and the dispersion was transferred to an Ar drybox. The minimum amount of anhydrous isopropanol required to precipitate the nanocrystals after centrifugation was added to the

dispersion. This prevented potential co-precipitation of the Cd-phosphonate complex. After removing the supernatant, the precipitate was re-dissolved twice in toluene and re-precipitated with isopropanol.

III. Device Fabrication. After synthesis, nanocrystals were dispersed in 20 mL pyridine and stirred under reflux overnight, allowing for comprehensive ligand exchange. Nanocrystals were then precipitated with hexane, washed with toluene, and redissolved in approximately one mL pyridine. These highly concentrated solutions were ultrasonicated for ca. 30 minutes and then passed through a 0.4 μm Teflon filter before spin-casting. Nanocrystal films were spin-cast at 1500-2000 rpm onto glass substrates coated with 150 nm ITO (Thin Film Devices Inc., resistivity 20 ohms/sq) and a high resistivity transparent layer of 2Å Al_2O_3 deposited by atomic layer deposition. To create bilayer structures, a single film was spin-cast and then heated for 15 minutes at 200 degrees C to remove excess solvent and allow for spin-casting of the second film. For sintering, a saturated solution of $CdCl_2$ in methanol was spin-cast onto standard bilayer samples at 1500rpm, afterwhich the samples were heated at 400 C in oxygen for 15 minutes. Finally, all samples were held at ca. 10^{-6} torr overnight, afterwhich top electrodes were deposited by thermal evaporation through a shadow mask, resulting in individual devices with 0.03 cm^2 nominal area.

III. Device Characterization. Simulated AM1.5G illumination was obtained with a Spectra Physics Oriel 300W Solar Simulator with AM1.5G filter set. The integrated intensity was set to 100 mW/cm^2 using a thermopile radiant power meter (Spectra Physics Oriel, model 70260) with fused silica window, and verified with a Hamamatsu

S1787-04 diode. Intensity was controlled to be constant throughout measurements with a digital exposure controller (Spectra Physics Oriel, model 68950). Short-circuit currents obtained under simulated AM1.5G illumination were well matched with those obtained by integrating EQE data with the true AM1.5G solar emission spectrum.